TECHNICAL **EBOOK**

Microstrip Antenna Design

Featuring Cadence AWR Software

This eBook explores microstrip antenna design, highlighting the single-element rectangular microstrip antenna and antenna arrays constructed from single microstrip elements.

Contents

MICROSTRIP ANTENNA DESIGN

$\vec{E} \times \vec{H}$ CONSULTING SERVICES

3 LITCHFIELD DRIVE

HAMPTON NH 03842-1564 USA

PREFACE

The material presented in this eBook comes from a technical tutorial written by Kenneth Puglia, principal at E x H Consulting Services, a company specializing in radar sensor systems, frequency synthesis, and frequency conversion. Kenneth is a former fellow of technology at M/A COM and a design engineer at Radio Corporation of America (RCA). He holds a BSEE from the University of Massachusetts and an MSEE from Northeastern University.

INTRODUCTION

A significant performance element in communication and radar systems, as well as wireless devices, is the antenna, which may be defined as a transducer between a guided electromagnetic (EM) wave propagating along a transmission line, and an EM wave propagating in an unbounded medium (usually free space) or vice-versa.[1] The antenna is required to transmit or receive EM energy with directional and polarization properties suitable for the intended application.

This eBook explores the radiation properties of rectangular microstrip antennas; specifically, the radiation method, coupling of the feed structure to the microstrip radiating element – or elements in the case of array structures – and the simple transmission line model utilized for design and performance estimates. In Part 1, the single element, rectangular microstrip antenna is explored. Part 2 examines the properties of antenna arrays constructed from the ensemble of single microstrip elements.

[1] Ulaby, F. T., *Fundamentals of Applied Electromagnetics*, 2004 Ed., Prentice Hall, Upper Saddle River, NJ, 2004.

CHAPTER I – SINGLE ELEMENT MICROSTRIP ANTENNA

ANTENNA CHARACTERIZATION

Antennas are characterized and described by classification and descriptive parameters. In addition to microstrip or printed antennas, other classes of antennas are: wire, e.g. dipole or loop; aperture, e.g. horns; reflector, e.g. parabolic; and lenses. The microstrip antenna may be considered a wire antenna due to the associated property of current on the radiating element; however, microstrip antennas are commonly granted the distinction of a separate antenna classification.

The most notable antenna parameters and definitions are summarized within Table 1.

TABLE 1: ANTENNA PARAMETERS AND DEFINITION[2]

PARAMETER	DEFINITION
Radiation Pattern	A mathematical function or graphical representation of the radiation properties of an antenna as a function of geometric, typically spherical, coordinates.
Radiation Pattern Beamwidth	The angular separation between two identical points on opposite sides of the radiation pattern maximum – generally, the value definition is the half-power point.
Sidelobe Level	The portion of the radiation pattern bounded by relatively weak radiation intensity
Directivity – D	The ratio of the radiation intensity in a given direction to the radiation intensity averaged over all directions – maximum radiation is the implied direction; a measure of the ability of the antenna to focus radiated power in a given direction
Gain – G	The ratio of the radiation intensity in a given direction to the radiation intensity of an isotropic antenna with the same input power – unlike directivity, gain also accounts for antenna efficiency
Efficiency – η	A numerical term which accounts for losses of the antenna from the input terminals and all elements of the antenna structure
Effective Area – A_e	The ratio of the available power at the terminals of an antenna to the power flux density from a plane wave incident normal to the antenna.
Aperture Efficiency	The ratio of the effective area, A_e, of an antenna to the physical area, A_{ph}, of the antenna – mathematically: $G = \frac{4\pi}{\lambda^2} \cdot A_e$ and $G = \frac{4\pi}{\lambda^2} \cdot \eta \cdot A_{ph}$
Polarization	Indicates the time varying direction of the electric field vector – vertical, horizontal and circular polarization are typical
Input Impedance	The ratio of voltage to current at the input terminals of the antenna

[2] Balanis, C. A., *Antenna Theory*, 3rd Ed., John Wiley and Sons, Hoboken, NJ, 2005, chapter 2.

In addition to the antenna definitions, understanding descriptive antenna parameters requires a graphical and geometric reference; that reference is provided by the spherical coordinate system as defined within Figure 1.

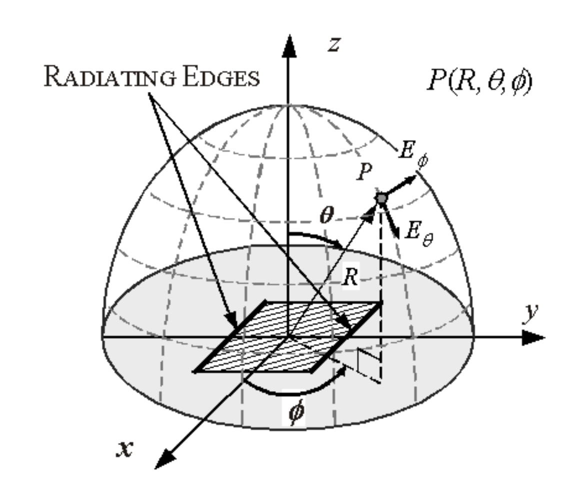

Figure 1 – Spherical Coordinate System

In the following discussion, geometric planes are referenced with respect to the graphic of Figure 1. Specifically, the E-plane (y-z) refers to the conditions: $\phi = \pi/2$ and $-\pi/2 < \theta < \pi/2$; while the H-plane (x-z) refers to the conditions: $\phi = 0$ and $-\pi/2 < \theta < \pi/2$.

The E-field and H-field of the radiated signal lie in the respective planes. Polarization of the radiated signal is defined with respect to the E-field.

For a microstrip antenna, radiation intensity is typically confined to the upper half hemisphere, i.e. above the *x*-y plane with radiation intensity in the positive *z*-direction.

MICROSTRIP ANTENNA DESCRIPTION

The microstrip, or patch, antenna is a relatively new development which was originally patented in 1955 but did not find broad application for almost two decades. Construction of a microstrip antenna embodies a dielectric substrate with ground plane conductor on one side and a thin, radiating conductor element on the opposite side as illustrated in Figure 2, where the radiating element is a rectangular conductor attached directly to a microstrip feed line.

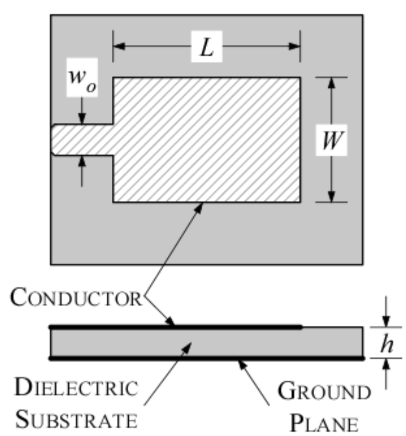

Figure 2 – Microstrip Antenna Construction

The principal attributes of microstrip antennas are summarized in Table 2.

TABLE 2: MICROSTRIP ANTENNA ATTRIBUTES[3,4]

POSITIVE ATTRIBUTE	**NEGATIVE ATTRIBUTE**
Low cost fabrication – printed circuit manufacturing methods	Narrow bandwidth – bandwidth increase generally requires increasing volume
Surface conformable – facilitated by flexible substrate materials	Sensitive to temperature and humidity – low loss substrates utilize PTFE in composite
Mechanically stable – dielectric substrates may use composite ceramic filled construction	Limitation on maximum gain
Polarization diversity – readily achieved using alternate feed methods	Poor cross polarization – limited element and feed isolation
Flexible gain and pattern options – readily achieved using alternate feed methods and array techniques	Spurious radiation – surface and other propagation modes
Ease of integration with other passive and active functions – achieved via compatibility with passive and active components	Low efficiency due to dielectric and conductor losses
Low profile – low profile planar construction	Modest power handling

In a properly designed microstrip antenna, the radiation intensity is in a direction normal to the radiating element, i.e. broadside. For the rectangular microstrip antenna, the length, L, is typically one-third to one-half wavelength long depending upon the substrate relative dielectric constant, which is commonly 2.0 to 10.0; the lower values of dielectric constant yielding higher efficiency.

The substrate height, h, is also a critical parameter with respect to efficiency and bandwidth, as well as reducing undesired propagation modes at the conductor edges and within the substrate.

There are several techniques available for the introduction of RF energy to the radiating microstrip via the feed line structure. In some cases, alterations in the feed line structure have the potential for attendant changes to the efficiency, gain and bandwidth of the microstrip antenna. The most common feed structure for the rectangular microstrip antenna is direct attachment at the radiating edge as illustrated.

The rectangular microstrip antenna geometry is most popular, however, alternate shapes, e.g. circular and triangular, provide utility in certain applications. Thin strips for the implementation of half-wavelength dipoles are attractive for increasing the operational bandwidth. To maintain brevity, the emphasis within this tutorial is restricted to microstrip antennas of rectangular geometry.

[3] Bancroft, R., *Microstrip and Printed Antenna Design*, 2nd Ed., Scitech Publishing, Raleigh, NC, 2009, pp. 5-6.

[4] Bahl, I. J. and Bhartia, P., Microstrip Antennas, Artech House, Dedham, MA, 1980, pp. 2-4.

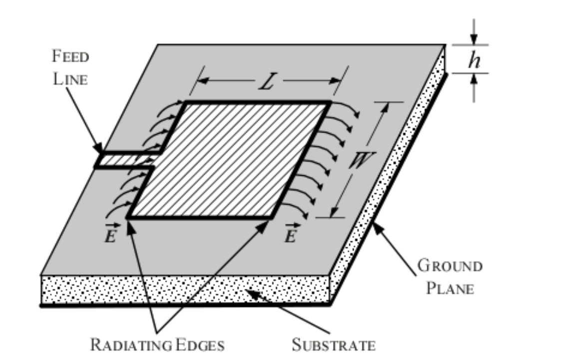

Figure 3 – Rectangular Microstrip Antenna – Radiating Edges

The graphic of Figure 3 represents the rectangular microstrip antenna with the various parameters identified. Note specifically the radiating electric field configuration at each edge of the microstrip conductor. Because the effective length of the microstrip conductor is a half-wavelength, the electric field is a maximum at the left and right edges due to the effective open-circuit and the repeating field pattern at half-wavelength intervals.

The radiation intensity is significantly influenced by the conductor length, L, and width, W, and to a lesser extent by the substrate height, h.

The microstrip conductor is located at the boundary of two dielectric materials: the substrate below the conductor and air above. Since part of the electric field is located within the substrate material and part in air, the relative dielectric constant of the substrate must be modified to accommodate the influence of the dielectric boundary. The accommodation is represented by the mathematical definition of the *effective* dielectric constant.

$$\varepsilon_{eff} = \frac{\varepsilon_r + 1}{2} + \frac{\varepsilon_r - 1}{2} \cdot \frac{1}{\sqrt{1 + \frac{12h}{W}}} \quad \text{for} \quad \frac{W}{h} > 1 \qquad \text{Eq. 1}$$

In addition to the influence of the dielectric substrate and air boundary, the impact of fringing of the electric field at the edges of the conductor must be accommodated. Electric field fringing at conductor edges may be accurately modeled by lumped element capacitors which effectively increase the electrical length of the conductor at each edge by an incremental length, ΔL. The incremental length is represented mathematically:[5]

$$\Delta L = 0.412 \cdot \frac{\left(\varepsilon_{eff} + 0.3\right)\left(\frac{W}{h} + 0.264\right)}{\left(\varepsilon_{eff} - 0.258\right)\left(\frac{W}{h} + 0.80\right)} \cdot h \qquad \text{Eq. 2}$$

Therefore, the effective, electrical length of the conductor may be written:

$$L_{eff} = L + 2\Delta L \qquad \text{Eq. 3}$$

As mentioned earlier, the electrical length of the microstrip conductor at resonance is $\lambda/2$. Therefore, accounting for the fringing, the resonant frequency, f_o, or corrected operating frequency, f_{rc}, may now be written:

$$f_o = \frac{c}{2\lambda} = \frac{c}{2 \cdot L_{eff} \cdot \sqrt{\varepsilon_{eff}}} = f_{rc} = \frac{c}{2\left(L + 2\Delta L\right)\sqrt{\varepsilon_{eff}}} \qquad \text{Eq. 4}$$

[5] Balanis, C. A., Antenna Theory, 3rd Ed., John Wiley and Sons, Hoboken, NJ, 2005, p. 818.

Transmission Line Model

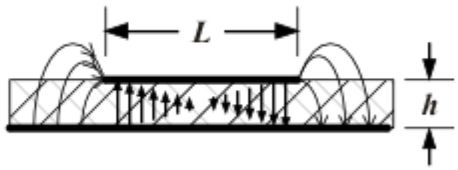

Figure 4 – Electric Field Distribution of Rectangular Microstrip Antenna

The rectangular microstrip antenna is uniquely represented by the transmission line model, which provides a simple analysis method as well as an intuitive understanding of the radiation mechanics and other operational parameters. It is also instructive to examine the relative magnitude of the E-field below the conductor in order to gain additional physical insight. To that end, Figure 4 is offered. Note specifically the E-field fringing at each end of the microstrip line as well as the dual dielectric occupancy mentioned earlier.

The transmission line model of the rectangular microstrip antenna utilizes an equivalent radiating slot of width W, and height h, to represent each of the radiating edges as graphically illustrated in Figure 5.

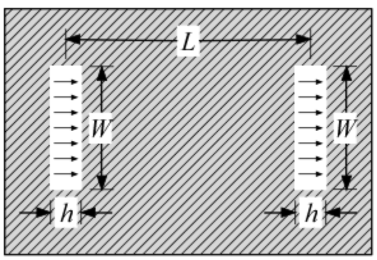

Figure 5 – Radiating Slot Equivalence to Microstrip Edges

Each slot may be represented by an equivalent admittance consisting of a conductance and susceptance:

$$Y = G + jB$$

The admittances are separated by a transmission line of length, L, and characteristic impedance, $Z_o = 1/Y_o$, thereby forming the equivalent network of the microstrip antenna as illustrated in Figure 6. The Equivalent circuit provides a convenient method of input impedance calculation upon numeric evaluation of the conductance and susceptance:[6]

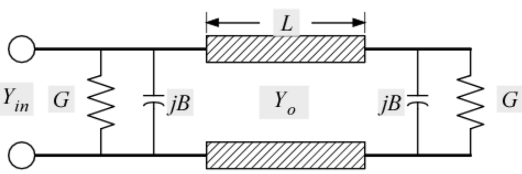

Figure 6 – Microstrip Antenna Equivalent Circuit

$$G = \frac{1}{120\pi^2} \cdot \left[1 - \frac{(k_o h)^2}{24}\right]$$

$$B = \frac{2\pi \Delta L \sqrt{\varepsilon_{eff}}}{\lambda_o Z_o}$$

$$Y_{in} = G + jB + Y_o \frac{G + j\left(B + Y_o \tan\left(k_o \sqrt{\varepsilon_{eff}} L\right)\right)}{Y_o + j(G + jB)\tan\left(k_o \sqrt{\varepsilon_{eff}} L\right)}$$

While the equations for the slot admittance are convenient, improved accuracy is achieved through the use of the equivalent admittance of the radiating slots available from the cavity model.

Cavity Model

Meticulous examination of the microstrip antenna construction discloses that the air dielectric at the sides and conductors at the top and bottom boundaries may define a resonant structure, also referred to as a resonant cavity. Cavity resonators are typically low loss structures; therefore, a mechanism must be defined to simulate the radiation loss at each edge of the microstrip conductor. Once again, the radiating slot finds application. However, in the case of the cavity model, the radiation admittance is evaluated from an electromagnetic field perspective of significant mathematical rigor which is not appropriate for this tutorial venue. Notwithstanding, the results of the cavity model are applicable and provide improved accuracy for the calculation of driving point impedance and

[6] Bahl, I. J. and Bhartia, P., Microstrip Antennas, Artech House, Dedham, MA, 1980, p. 51.

resonant frequency.[7] Utilization of the cavity model yields the following equations for the calculation of the resonant input resistance of the rectangular microstrip resonator:[8] Note that the ± sign refers to the specific mode field configuration of the cavity resonance beneath the conductor [3].

$$R_{in} = \frac{1}{2(G_1 \pm G_{12})} \qquad \text{Eq. 5}$$

$$G_1 = \frac{I_1}{120\pi^2} \quad \text{where} \quad I_1 = \int_0^{\pi} \left[\frac{sin\left(\frac{k_o W}{2}\right) cos\theta}{cos\theta} \right]^2 \cdot sin^3(\theta) d\theta$$

$$G_{12} = \frac{1}{120\pi^2} \cdot \int_0^{\pi} \left[\frac{sin\left(\frac{k_o W}{2} cos\theta\right)}{cos\theta} \right]^2 \cdot J_0(k_o L \sin\theta) sin^3\theta \cdot d\theta$$

Microstrip Antenna Feed Line

The resonant input resistance at the edge of the microstrip conductor is generally greater than the feed line characteristic impedance and requires an impedance matching structure in order to reduce the mismatch loss and thereby improve the antenna efficiency. There are two common feed line techniques which facilitate the impedance matching required to achieve an efficient rectangular microstrip antenna as illustrated in Figure 7.

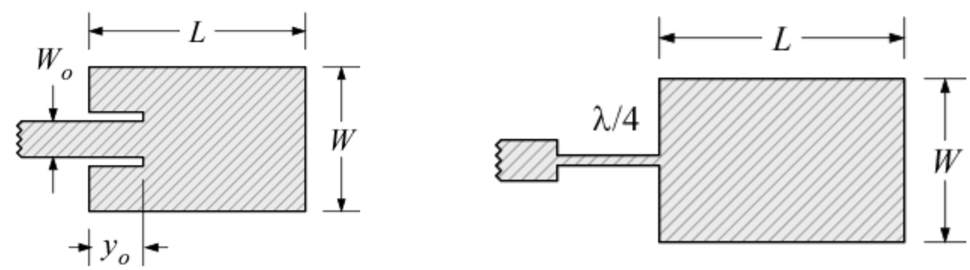

a. Inset Feed Matching **b. Quarter Wavelength Matching**

Figure 7 – Impedance Matching Feed Line Techniques

The inset feed technique utilizes the reduction in electric field strength to effectively 'tap' a lower impedance drive point, while the quarter-wave transformer uses the transmission line formula which provides the geometric mean of the input resistance and the characteristic impedance of the quarter-wave transmission line. Coaxial probes beneath the conductor or a vertically offset feed along the width are also used on occasion.

A useful equation to achieve the optimum inset length, y_o, is available:[9]

$$R_{in}(y = y_o) = \frac{1}{2(G_1 + G_{12})} \cdot cos^2\left(\frac{\pi}{L} y_o\right) = R_{in}(y_o = 0) \cdot cos^2\left(\frac{\pi}{L} y_o\right) \qquad \text{Eq. 6}$$

Although quite convenient and easily implemented, the inset feed distorts the equivalent slot radiation due to the change in geometry. The quarter-wavelength feed minimizes the equivalent slot field distortion due to the

[7] The diligent readers are encouraged to indulge their curiosity in one or more of the cited references.

[8] Although the expressions appear quite complex, they are rendered tractable using computational programs such as MathCad® and Matlab®. The data analysis feature of Excel may also be employed to provide a reasonable estimate.

[9] Balanis, C. A., Antenna Theory, 3rd Ed., John Wiley and Sons, Hoboken, NJ, 2005, pp. 824-825.

narrower, high impedance line required for impedance matching. The simple formula for the impedance of the quarter-wavelength transmission line may be written:

$$Z_{in} = \frac{Z_o^2}{R_{in}} \qquad \text{Eq. 7}$$

For a typical value of R_{in} = 200 Ω and Z_{in} = 50 Ω:

$$Z_o = \sqrt{R_{in} \cdot Z_{in}} = \sqrt{200 \cdot 50} = 100\ \Omega \qquad \text{Eq. 8}$$

Radiation Intensity Patterns

The two-slot radiation model is utilized in predicting the E-plane and H-plane radiation patterns. The radiation intensity of the rectangular microstrip antenna of width W, length L, and height h, may be calculated using the following equations:[10]

For the *E*-plane radiation pattern: $\phi = 0$ and $-\pi/2 < \theta < \pi/2$ (planes have been redefined to comply with reference)

$$P_E(\theta, \phi = 0) = cos\left(\frac{k_o h}{\sqrt{\varepsilon_r}} \cdot cos(\theta)\right) \cdot \frac{sin\left(\frac{k_o W}{2} \cdot sin(\theta) \cdot sin(\phi)\right)}{\frac{k_o W}{2} \cdot sin(\theta) \cdot sin(\phi)} \cdot cos\left(\frac{k_o L}{2} \cdot sin(\theta) \cdot cos(\phi)\right) \cdot cos(\phi),\ k_0 = \frac{2\pi}{\lambda_0} \qquad \text{Eq. 9}$$

For the *H*-plane radiation pattern: $\phi = \pi/2$ and $-\pi/2 < \theta < \pi/2$ (planes have been redefined to comply with reference)

$$P_H\left(\theta, \phi = \frac{\pi}{2}\right) = cos\left(\frac{k_o h}{\sqrt{\varepsilon_r}} \cdot cos(\theta)\right) \cdot \frac{sin\left(\frac{k_o W}{2} \cdot sin(\theta) \cdot sin(\phi)\right)}{\frac{k_o W}{2} \cdot sin(\theta) \cdot sin(\phi)} \cdot cos\left(\frac{k_o L}{2} \cdot sin(\theta) \cdot cos(\phi)\right) \cdot cos(\theta) \cdot sin(\phi),\ k_0 = \frac{2\pi}{\lambda_0} \qquad \text{Eq. 10}$$

Bancroft[11] provides reduced complexity expressions for the E-plane and H-plane radiation patterns; however, accuracy is modestly compromised due to elimination of the height, h, as a dependent variable.

Microstrip Antenna Directivity

The two-slot radiation model is also utilized to predict the directivity of the rectangular microstrip antenna. Figure 5 represents graphic definition in conjunction with the microstrip antenna dimensions as previously defined. Although the equation for directivity of a single slot requires the condition $k_o h \ll 1$, the expression provides reasonable accuracy upon comparison with actual measurement if the condition is moderately violated.

The directivity of a single slot may be written:[12]

$$D_1 = \left(\frac{2\pi W}{\lambda_o}\right)^2 \cdot \frac{1}{I_1} \quad \text{where} \quad I_1 = \int_0^\pi \left[\frac{sin\left(\frac{k_o W}{2}\right) cos\,\theta}{cos\,\theta}\right]^2 \cdot sin^3(\theta) d\theta \qquad \text{Eq. 11}$$

The directivity of a two-slot array, i.e. the microstrip antenna, may be written using the following expression:[13]

[10] Carver, K. and Mink, J., Microstrip Antenna Technology, IEEE Transactions, Antennas and Propagation, January, 1981.

[11] Bancroft, R., *Microstrip and Printed Antenna Design*, 2nd Ed., Scitech Publishing, Raleigh, NC, 2009, p. 30.

[12] Balanis, C. A., Antenna Theory, 3rd Ed., John Wiley and Sons, Hoboken, NJ, 2005, p. 840.

[13] Balanis, C. A., Antenna Theory, 3rd Ed., John Wiley and Sons, Hoboken, NJ, 2005, p. 841.

$$D_2 = \left(\frac{2\pi W}{\lambda_o}\right)^2 \cdot \frac{\pi}{I_2}$$

$$\text{where } I_2 = \int_0^{\pi}\int_0^{\pi}\left(\frac{\sin\left(\frac{k_o W}{2}\cdot\cos(\theta)\right)}{\cos(\theta)}\right)^2 \cdot \sin^3(\theta)\cdot\cos^2\left(\cos\left(\frac{k_o L_{eff}}{2}\right)\cdot\sin(\theta)\cdot\sin(\phi)\right)d\theta d\phi \qquad \text{Eq. 12}$$

Microstrip Antenna Design

Although the previous text and equations have indicated a significant performance dependence on the width of the microstrip conductor, the astute reader may recognize that no guidelines or formulae have been offered for the width calculation. A practical starting point has been suggested by Bancroft in the following equation:[14]

$$W = \frac{c}{2f_o}\cdot\sqrt{\frac{2}{\varepsilon_r + 1}} \qquad \text{Eq. 13}$$

The procedure for the design of a single element, rectangular microstrip antenna is summarized in Table 3.

Table 3: Microstrip Antenna Design Procedure

Procedure Number	Design Procedure Description	Note – Comment – Reference
1.	Specify: A. substrate dielectric constant – ε_r B. operational frequency – f_o C. substrate height – h	A. Preferred values of dielectric constant 2.0 < ε_r < 6. Higher dielectric constants reduce efficiency B. Desired center frequency C. substrate height should be compatible with achievable line width and impedance levels Bancroft recommends: $h_{max} < \frac{0.3c}{2\pi f_o\sqrt{\varepsilon_r}}$
2.	Calculate the width – W	Equation 13.
3.	Calculate the effective dielectric constant – ε_{eff}	Equation 1.
4.	Calculate the length extension – ΔL	Equation 2.
5.	Calculate the actual length – L	Equation 4. Note the terms must be rearranged to solve for L. L is nominally a half-wavelength in the effective dielectric medium
6.	Calculate the input impedance at resonance – R_{in}	Equation 5.

[14] Bancroft, R., Microstrip and Printed Antenna Design, 2nd Ed., Scitech Publishing, Raleigh, NC, 2009, p. 60.

Procedure Number	**Design Procedure Description**	**Note – Comment – Reference**
7.	Use either inset feed or quarter-wavelength transmission line for impedance matching to the desired input impedance	Equation 6 or Equation 7. A coaxial probe beneath the substrate with center conductor extending to the inset feed point may also be appropriate on occasion.
8.	Calculate the directivity	Equation 12
9.	Calculate the radiation patterns	Equation 9 and Equation 10
10.	Simulate antenna design using an EM simulator and compare results	EM simulation tools have provided accurate performance predictions and in many cases have expedited the design cycle time by limiting the prototype fabrication stage to a single iteration.
11.	Fabricate antenna and compare measured results with design and simulation	

Microstrip Antenna Design Example

To summarize the rectangular microstrip antenna tutorial content at this point:

- Operational parameters and principles have been established
- Design parameters and equations have been presented and references identified
- Design procedure has been outlined

To further explore the rectangular microstrip antenna, a design example is documented in Table 4 using the procedure of Table III. The example illustrates the design procedure for a 5.8 GHz, direct coupled microstrip antenna on 0.062-inch-thick Rexolite® substrate. Rexolite is a dimensionally stable, cross-linked polystyrene plastic with a frequency independent dielectric constant of 2.55 and low loss tangent; typically less than 0.001 to 100 GHz.[15]

Table 4: Microstrip Antenna Design Example

Design Parameter	**Symbol**	**Design Value**	**Note – Comment**
Center Frequency	f_o	5.8 GHz	Operational frequency
Dielectric Constant	ε_r	2.55	Specified parameter
Substrate Height	h	1.575 mm (0.062 in)	Specified parameter
Conductor width	W	19.41 mm (0.764 in)	Equation 13
Effective dielectric constant	ε_{eff}	2.327	Equation 1

[15] Additional information and characteristics of Rexolite may be found at www.rexolite.com.

Design Parameter	**Symbol**	**Design Value**	**Note – Comment**
Length extension	ΔL	0.79 mm (0.031 in)	Equation 2
Conductor length	L	15.38 mm (0.605)	Equation 4
Resonant input resistance	R_{in}	248 Ω	Equation 5
Inset feed length	y_o	5.41 mm (0.213 in)	Equation 6
Quarter-Wave transformer	Z_o	112 Ω	Equation 7
Quarter-Wave transformer	$L_{\lambda/4}$	8.48 mm (0.334 in)	Microstrip calculator[16]
Quarter-Wave transformer, width	$W_{\lambda/4}$	1.05 mm (0.035 in)	Microstrip calculator[16]
Directivity	D	7.0 dB	Equation 12
Radiation pattern E-plane	P_E	Figure 8	Equation 9
Radiation pattern H-plane	P_H	Figure 8	Equation 10

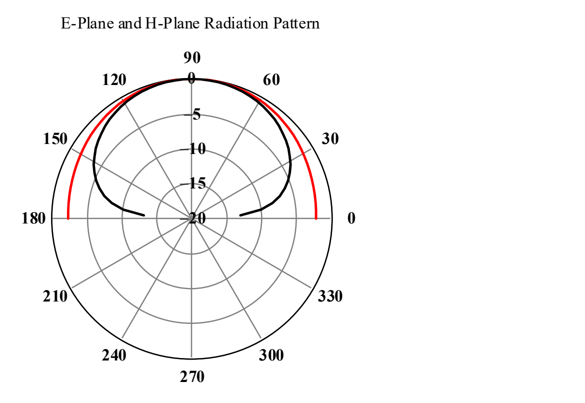

Figure 8 – E-Plane (red) and H-Plane (black) Radiation Patterns

Figure 8 represents the E-plane and H-plane radiation patterns of the 5.80 GHz, rectangular microstrip antenna. Note that the beamwidth of the E-plane radiation pattern is somewhat greater than the H-plane beamwidth. It should also be noted that the H-plane radiation pattern is independent of the slot separation length, L; this is not evident from equation 10 until one cautiously considers the equation under the condition, $\phi = \pi/2$.

The E-plane and H-plane radiation patterns of Figure 8 were calculated with MathCad™ using the equations of [4]. Similar patterns are produced using the other cited references.

[16] On-Line microstrip parameter calculator: http://www.microwaves101.com/content/calculators.cfm

ELECTROMAGNETIC SIMULATION OF DIRECT COUPLED MICROSTRIP ANTENNA

Although the design equations provide the initial dimensional data and radiation patterns for the microstrip antenna design, an EM simulation is generally required to reduce the number of prototype iterations and to achieve the available performance objectives. To that end, an EM simulation of the 5.8 GHz, direct coupled microstrip antenna was executed using the NI QAWR Design Environment AXIEM planar EM simulator.[17]

Results of the direct-coupled microstrip antenna electromagnetic simulation are summarized within the graphics of Table 5 and represent a degree of dimensional optimization of the initial design values as previously indicated.

TABLE 5: ELECTROMAGNETIC SIMULATION RESULTS

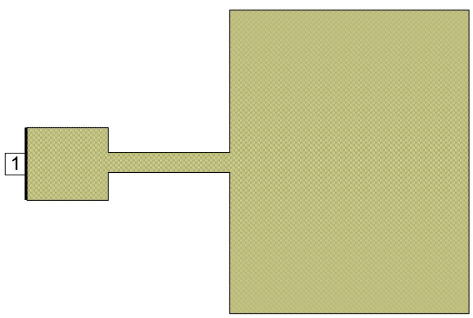

Microstrip Antenna Conductor Pattern

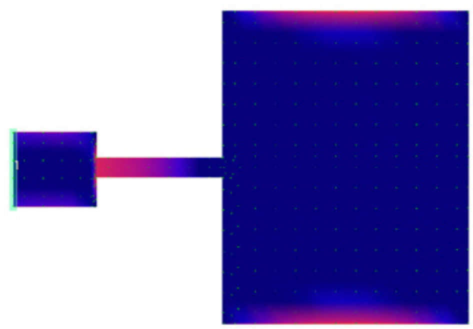

Conductor Current Distribution

(note the concentration of current at the top edges of the conductor)

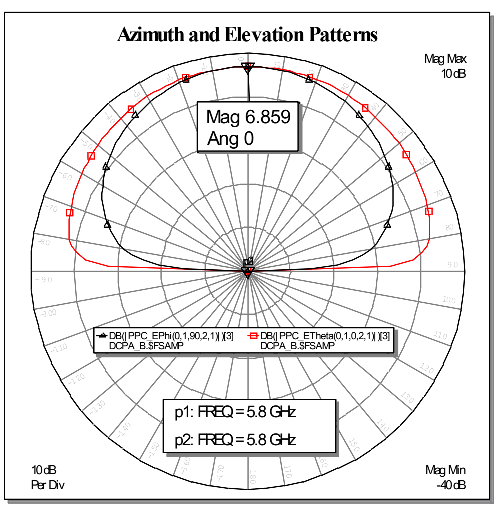

Azimuth (E-Plane) and Elevation (H-Plane) Radiation Patterns

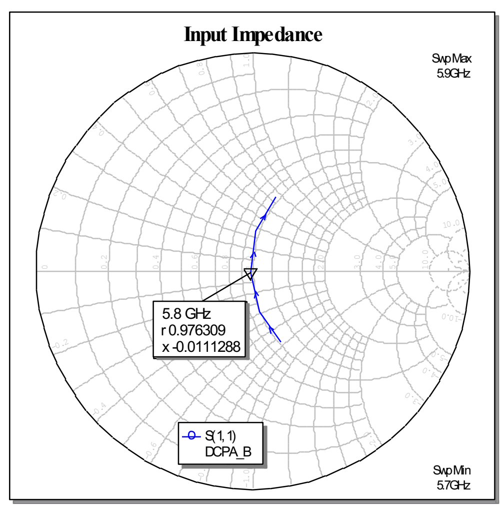

Direct-Coupled Microstrip Antenna Input Impedance

In addition to providing the ability to optimize antenna performance, the AXIEM simulation software also enables dimensional sensitivity analysis; e.g., as one might expect, the length of the microstrip conductor (L) was found to

[17] AXIEM technology utilizes an open-boundary, non-gridded, method-of-moments (MoM) solver that supports thick metal in layered dielectric media. Additional information is available at https://www.awr.com/software/products.

significantly influence input impedance, directivity and center frequency; while the microstrip conductor width (W) was found to have only modest influence on the directivity but was useful in optimizing the input impedance. The substrate thickness (h) was found to be the principal determinant to bandwidth.

The value of EM antenna simulation is manifest in the ability to optimize performance as well as to provide physical insight to antenna operation using conductor current and electric field annotation capabilities. Note specifically the current density at the conductor edges. One might correctly consider that the radiation properties of the microstrip antenna may also be explored using the current density; in fact, the radiation patterns of the microstrip antenna could also be calculated using the vector potential associated with the conductor current.

PROTOTYPE MICROSTRIP ANTENNA

A prototype microstrip antenna was fabricated in accordance with the parameters of Table IV with modest dimensional revision resulting from the EM simulation to optimize the input impedance and directivity. The prototype antenna conductor dimensions and photograph are illustrated in Figure 9.

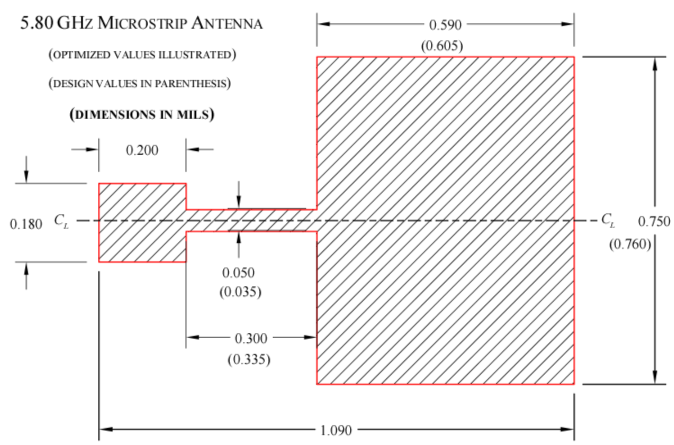

a. Microstrip Antenna Conductor Pattern

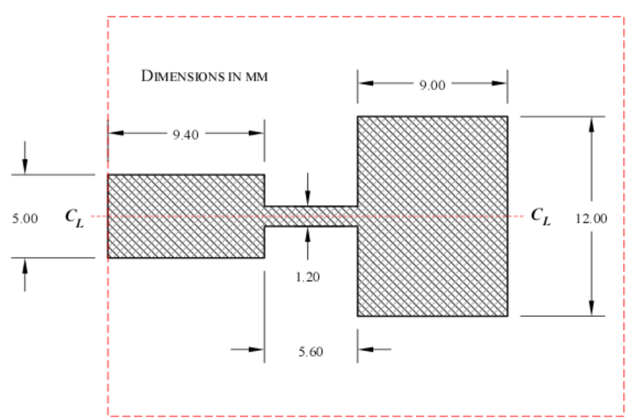

b. Photograph – PLACE HOLDER

Figure 9 – Prototype Microstrip Antenna

CHAPTER 2 – INTRODUCTION TO MICROSTRIP ANTENNA ARRAYS

MICROSTRIP ANTENNA ARRAY

Although there are a significant number of applications for the single element microstrip antenna, in many cases, the performance enhancements and features of multiple microstrip element arrays add to an expanding list of new opportunities. A microstrip antenna array is formed by the arrangement, or grouping, of multiple, single-element microstrip antennas. The respective geometric positioning of the individual elements, as well as the element amplitude and phase excitation, determines the characteristics of the antenna array. Microstrip antenna arrays are typically designed to enhance the antenna performance beyond that available from a single element; for example, arrays of single-element microstrip antennas offer increased gain and narrower beamwidth at the cost of larger aperture area. In addition, array antennas also offer the ability to steer the principal radiation intensity beam via differential phase excitation and to reduce sidelobe levels by variable power excitation to the individual elements of the array – properties which compel emphasis in many applications.

The individual dimensional elements of a microstrip antenna array may vary and may be spatially configured in a linear, planar or volumetric arrangement. The radiation pattern of an array is determined by the dimensions, spatial distribution and electrical excitation, i.e., amplitude and phase, of the individual elements. Given the number of variables, a general approach to the synthesis and design of antenna arrays is clearly required. To that end, antenna specialists have been successful in formulating a general methodology using the following definitions:

ANTENNA ARRAY TERM	**ANTENNA ARRAY DEFINITION**
Array Factor (*AF*)	The array factor defines the radiation pattern of spatially distributed isotropic radiating elements in accordance with the amplitude and phase of element excitation. The array factor is a function of the number, dimensional spacing, and the amplitude and phase of the excitation signal of the elements.
Element Factor (*EF*)	The element factor is the radiation pattern of the individual elements of an array.

The product of the array factor and the element factor is referred to as the pattern multiplication theorem. An example will illustrate the convenience and efficiency of the theorem.

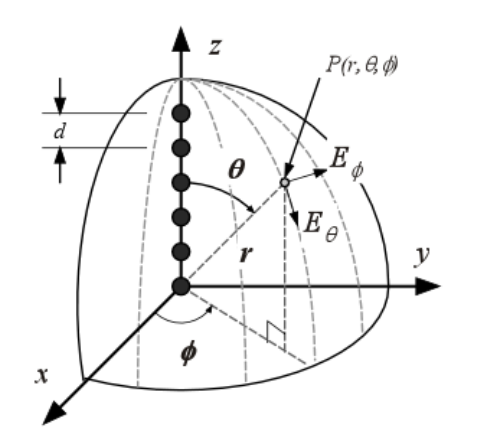

Figure 10: Linear Array of Isotropic Radiating Elements

Consider the linear distribution of equally spaced, isotropic radiating elements along the *z*-axis as shown in Figure 10. The *E*-field radiation pattern of the i^{th} element may be written:[18]

$$E_i(\theta,\phi) = F(\theta,\phi) \cdot I_i \, exp\left[j\left(k_0 z_i \cos\theta + \beta_i\right)\right]$$

The following definitions are applicable to this equation:

$F(\theta,\phi)$ – represents the radiation pattern of the element, and $k_0 = 2\pi/\lambda_0$, I_i and β_i are the amplitude and phase excitation.

For n identical elements, the radiation pattern is written:

$$E(\theta,\phi) = F(\theta,\phi) \cdot \sum_{i=0}^{n-1} I_i \, exp\left[j\left(k_0 z_i \cos\theta + \beta_i\right)\right]$$

[18] Bahl, I. J. and Bhartia, P., Microstrip Antennas, Chapter 7, Artech House, Dedham, MA, 1980

The radiation pattern is the product of the two terms:

$F(\theta,\phi)$ – is the element factor, EF, and, $\sum_{i=0}^{n-1} I_i \, exp\left[j\left(k_0 z_i \cos\theta + \beta_i\right)\right]$ is the array factor, AF.

The perceptive reviewer may recognize the similarity of the array factor to the discrete Fourier transform of the complex linear distribution of amplitude and phase of the radiating elements. For the specified equally spaced condition and progressive phase of each element, one may write:

$z_i = 0, d, 2d \ \ldots \ (n-1)d$ and $\beta_i = 0, \beta_0, 2\beta_0 \ \ldots \ (n-1)\beta_0$

If the indicated substitutions are implemented, the array factor may be written:

$$AF(\theta) = \sum_{i=0}^{n-1} I_i \, exp\left[j\left(\frac{2\pi}{\lambda_0} i \cdot d \cos\theta + i \cdot \beta_0\right)\right]$$

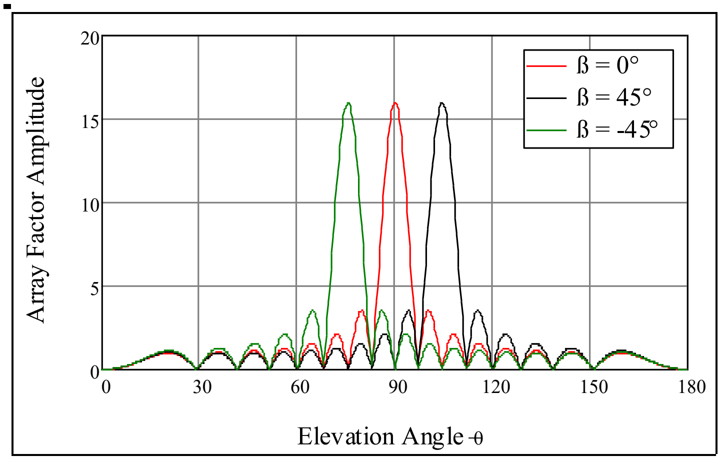

Figure 11: Array Factor for Linear Array of Isotropic Elements

Solution of the equation using constant amplitude distribution (I_i = 1.0), parametric phase progression, (β_0 = 0, β_0 = -π/4, β_0 = π/4), number of elements (n = 16) and element spacing (d = λ_0/2), the graphic results of Figure 12 are disclosed.

The maximum amplitude of the array factor occurs at θ = 90° for 0° phase excitation; at 105° for 45° phase progression; and at 75° for -45° phase progression. Clearly, the phase progression excitation enables the significant property of main beam steering of antenna arrays. An additional observation is that the array of isotropic radiating elements has provided focus, i.e. gain, over the single element; in this instance, the gain is equal to the number of array elements, n.

Another observation from Figure 11, is the sin(x)/x amplitude function; this behavior might have been anticipated due to the constant amplitude element excitation and the discrete Fourier transform relationship.

Constant, or uniform, amplitude distribution has been considered to this point of the exercise; however, in addition to phase progression excitation, amplitude variation of the array elements also offers some interesting properties. Consider the graphic of Figure 12, where the array factor for constant amplitude element excitation is indicated in a., while raised cosine element amplitude excitation has been implemented in b.

The raised cosine amplitude excitation of the array elements has significantly reduced the array sidelobes; unfortunately, the array amplitude has also been reduced and the beamwidth increased. These are the major trade-offs when considering application of the antenna array.

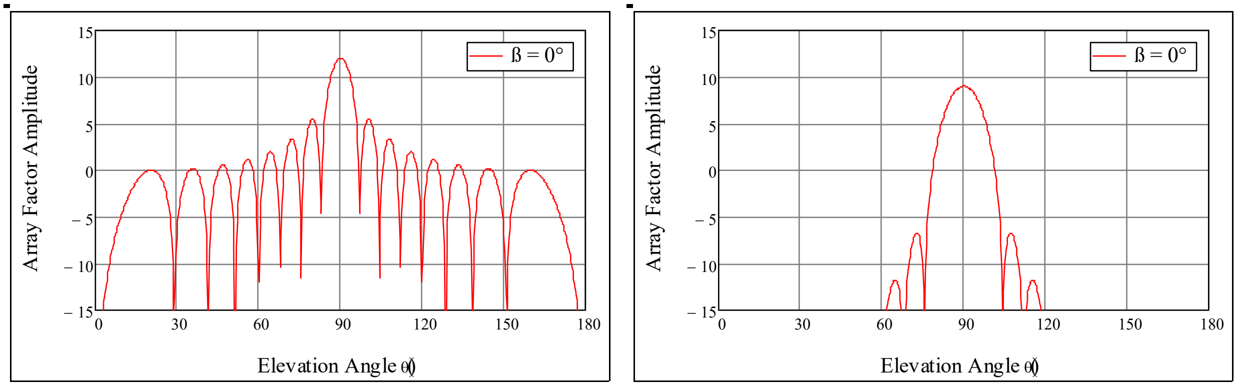

a. Constant Amplitude Excitation **b. Cosine Amplitude Excitation**

Figure 12: Array Factor versus Element Amplitude Variation (note logarithmic amplitude scale)

Microstrip antenna arrays will be further explored within the electromagnetic simulations of the following sections. In many instances, the element spacing for most applications is approximately half-wavelength ($\lambda_0/2$) in air. Although somewhat higher gain may be attained, using element spacing beyond half-wavelength produces high sidelobe levels, particularly near ±90° off boresight. Therefore, in the simulations to follow, element spacing in the plane of the antenna will be approximately half-wavelength.

Linear Microstrip Array Antennas

Figure 13 illustrates the configuration of a parallel feed – alternately referred to as corporate feed – linear array composed of four, in-line elements. Each element of the linear array is fed from the output of a power divider which facilitates excitation of either equal or unequal power to each element. The power distribution to the elements of an array, as previously indicated, is commonly referred to as amplitude taper and is utilized to reduce sidelobe levels. Unequal amplitude taper is accompanied by main beamwidth extension and reduced gain with respect to uniform, or equal, power distribution to each element.

The excitation to each element of the array may also be varied in phase. Progressive differential phase excitation is employed to steer the main beam off-boresight, and is a unique and attractive feature for large phased array radar applications as an alternative to inertial (mechanical) platforms.

A four element linear array has been constructed using the single element, 5.80 GHz microstrip antenna previously described and analyzed. The data from EM analysis of the four element array is summarized in Table VI below.

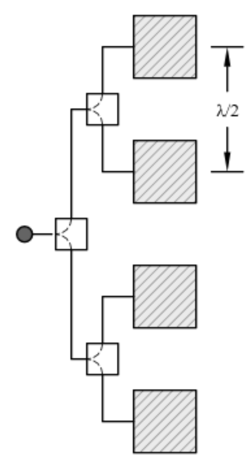

Figure 13: Four-Element Linear Array

TABLE VI: PERFORMANCE OF FOUR-ELEMENT LINEAR ARRAY

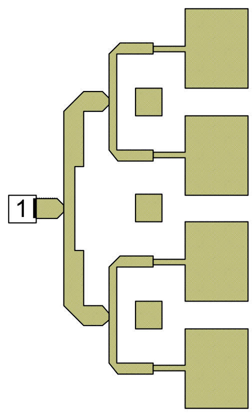

Four-Element Linear Array Conductor Pattern
(equal amplitude and phase to each element)

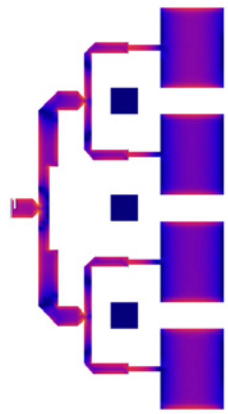

Four-Element Linear Array Conductor Current[19]
(note equal amplitude and phase excitation)

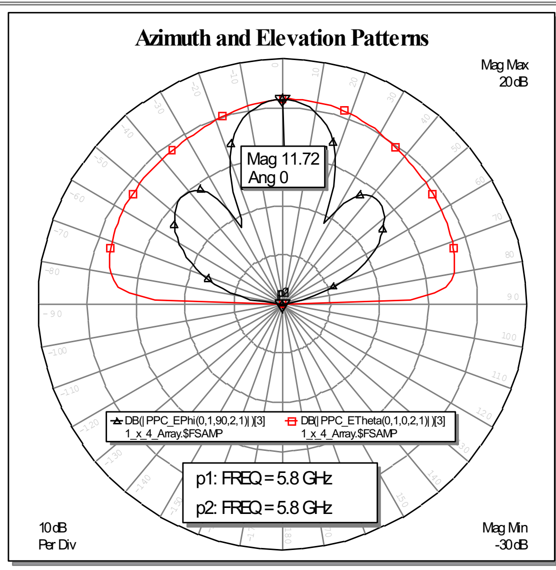

Four-Element Linear Array Radiation Patterns
(note increased gain, EL beamwidth reduction and sidelobes)

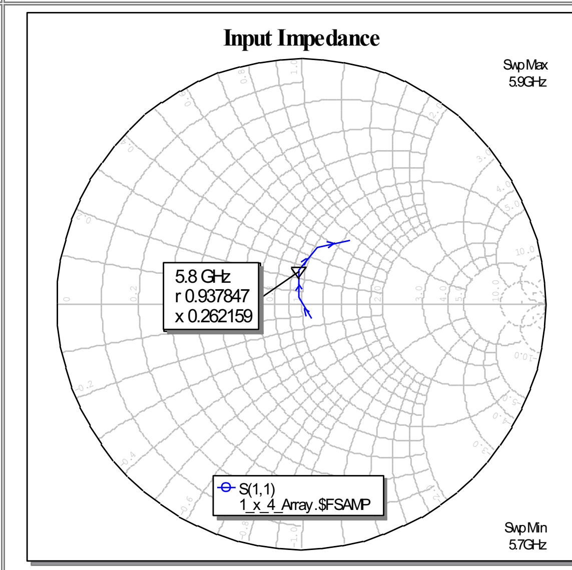

Four-Element Linear Array Input Impedance
(note increase in impedance bandwidth versus single element)

TABLE 6 documents the performance of a Four-element linear array to which an amplitude taper has been applied. As mentioned previously, the amplitude taper is utilized to reduce sidelobe levels. The amplitude taper is implemented by changes to the impedance of the lines of the power divider in a manner that alters the impedance at the principal junction of the power divider. A simple equation governs the power divider design under the specified conditions.[20]

[19] The current density annotation feature available within the AXIEM EM analysis software provides significant physically insightful information. The graphic indicates that the amplitude and phase of the individual element excitation are equal. This feature is uniquely valuable in evaluation of proper amplitude and phase excitation of more complex array structures.

[20] The unequal power divider is documented at the website: http://www.microwaves101.com/encyclopedia/calpowerdivider.cfm

TABLE 6: PERFORMANCE OF FOUR-ELEMENT LINEAR ARRAY WITH AMPLITUDE TAPER

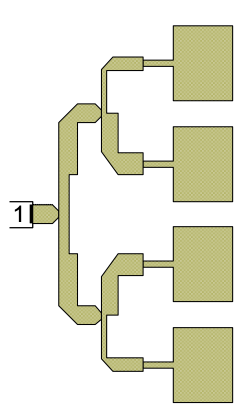 **Four-Element Linear Array Conductor Pattern** (note power divider line impedance difference)	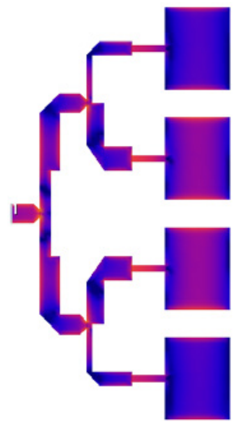 **Four-Element Linear Array Conductor Current**[21] (note unequal amplitude and equal phase excitation)
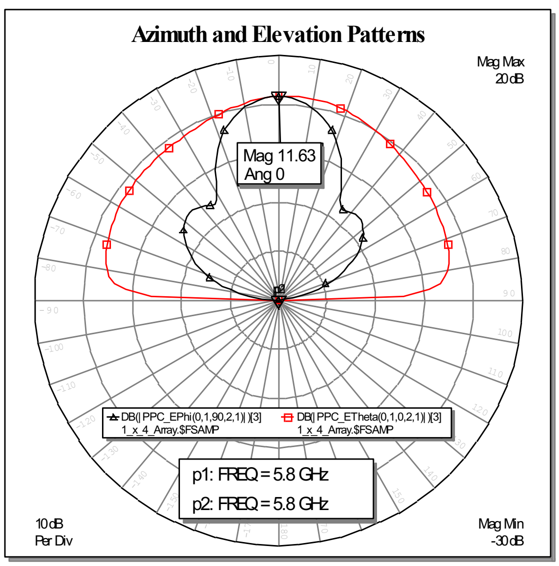 **Four-Element Linear Array Radiation Patterns** (note reduction to sidelobes versus equal amplitude)	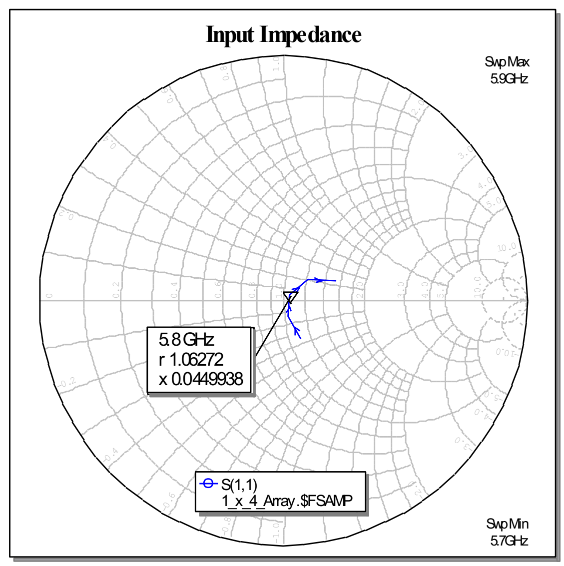 **Four-Element Linear Array Input Impedance** (note increase in impedance match bandwidth over single element)

Table 7 illustrates the configuration of a two-x-two array. The two-x-two array excitation is generally uniform and the feature most prominent is that the gain is typically 6 dB above the single element configuration with the commensurate reduction in *E*-plane and *H*-plane beamwidth. In this case, the gain, 11.45 dB, is limited due to the inclusion of line and impedance mismatch loss. The conductor current discloses that each element of the array is uniformly excited in amplitude and phase.

[21] The current density annotation feature available within the AXIEM EM analysis software provides significant physically insightful information. The graphic indicates that the amplitude and phase of the individual element excitation are equal. This feature is uniquely valuable in evaluation of proper amplitude and phase excitation of more complex array structures.

The differential feed at the center of the conductor pattern may be implemented from a balun located below the plane of the array. Differential feed is required in this case due to the inverse polarity of the radiating edges. The input impedance is 100 Ohms at the center frequency which is commensurate with typical balun impedance.

TABLE 7: PERFORMANCE OF TWO-X-TWO MICROSTRIP ANTENNA ARRAY

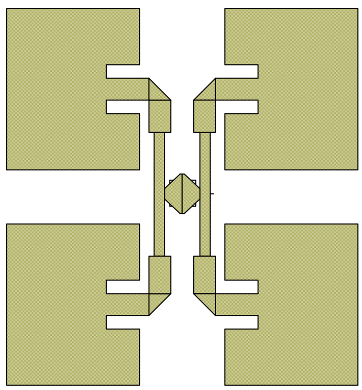

Two x Two Array Conductor Pattern

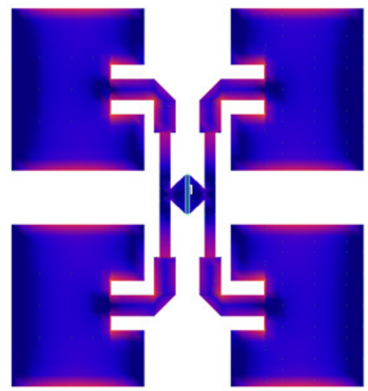

Two x Two Array Conductor Current

(note equal phase and amplitude excitation)

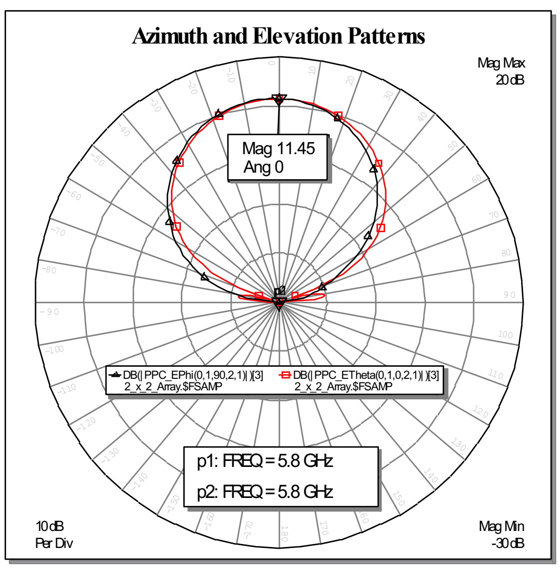

Two x Two Array Radiation Patterns

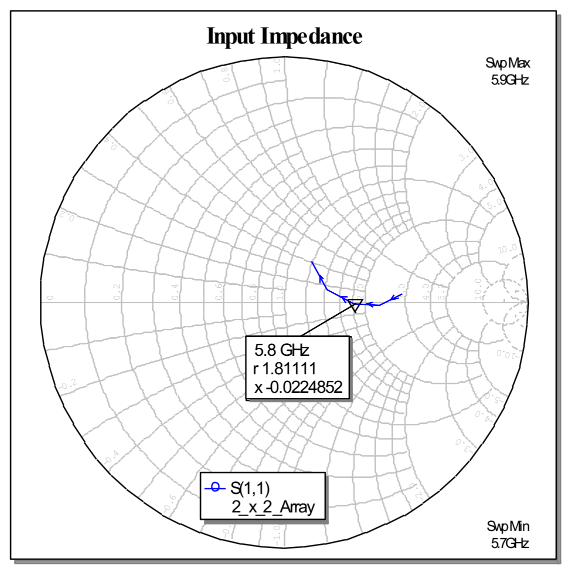

Two x Two Array input impedance

The individual excitation parameters of amplitude and phase determine the principal radiation intensity beamwidth, gain, direction and sidelobe level. Clearly, antenna arrays are significant performance determinants to communication and radar systems.

SERIES FEED FOR MICROSTRIP ARRAY ANTENNAS[22]

In addition to the parallel, or corporate, feed for microstrip antenna arrays, the series feed offers an additional method of array implementation. The microstrip array series feed is illustrated in Figure 11 where an *N*-element

[22] The series fed array is also referred to as a traveling wave antenna.

array is depicted as well as a five-element array featuring the ease with which amplitude taper may be implemented.

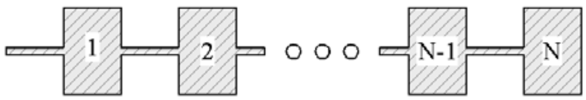

a. N-Element Series Feed Microstrip Array

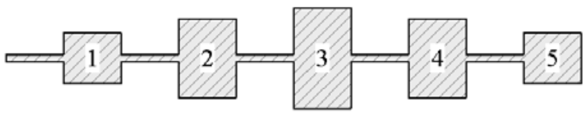

b. 5-Element Series Feed Microstrip Array with Amplitude Taper

Figure 14: Series Feed Microstrip Array

Recall from the introductory material that the width, W, of the conductor is a determining factor with regard to directivity and impedance.[23]

It is also instructive to view the equivalent circuit of the series arrangement in combination with admittance elements developed from the transmission line and cavity models, as illustrated in Figure 15.

The equivalent circuit has demonstrated utility in providing reasonable initial values for the element dimensions and the connecting line impedance.

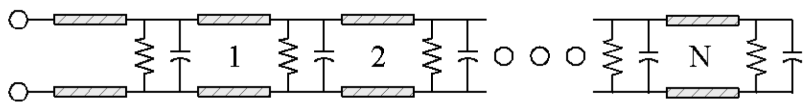

Figure 15: Series Feed Microstrip Array

Using the single element microstrip antenna initially investigated and empirical adjustment of element width to produce an amplitude taper, a 1-x-5 array has been constructed and an EM analysis executed. The results are graphically illustrated in Table 8.

[23] See equations 5 and 12.

Table 8: 1-x-5 Element Linear Array

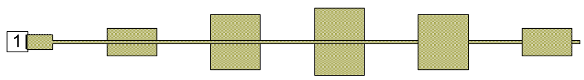 **a. 1-x-5 Linear Array with Amplitude Taper** During a sequence of simulations, the width of each element was adjusted to reduce the sidelobe levels to acceptable limits; in this case, -20 dB.	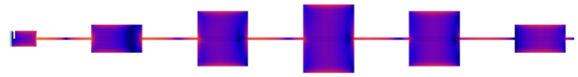 **b. Conductor Current Distribution** The conductor current distribution illustrates amplitude taper and near 0° phase progression. The slight difference in the excitation phase contributes asymmetry to the radiation pattern.
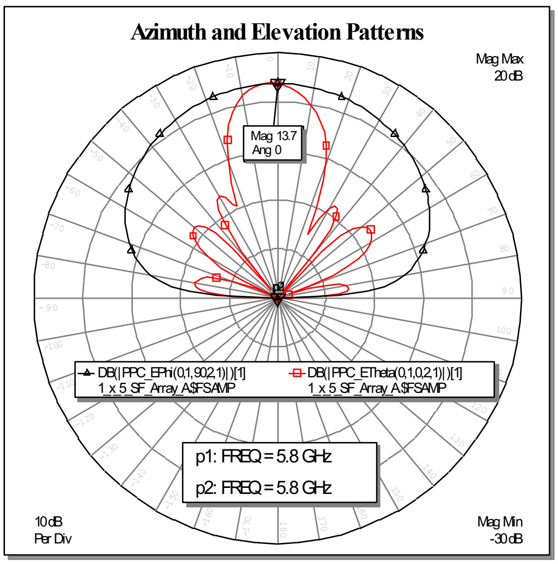 **c. 1-x-5 Array Radiation Patterns** The azimuth and elevation radiation patterns exhibit a perceptible asymmetry due to minor unequal phase excitation. Ideally, the on-boresight gain would be 14 dB; however, conductor losses have modestly reduced the gain to 13.7 dB.	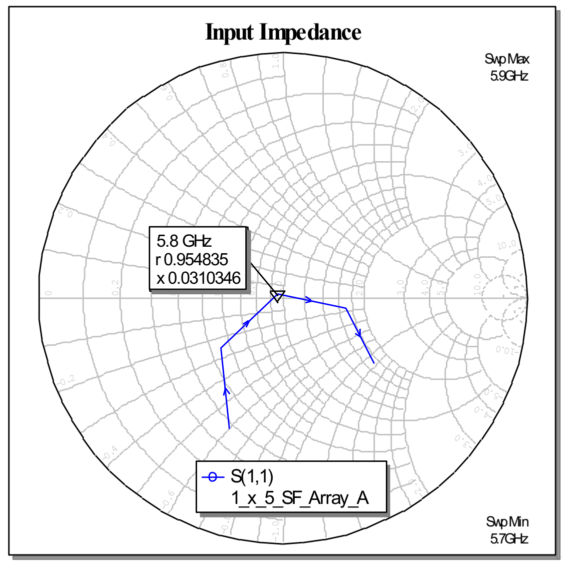 **d. 1-x-5 Array Input Impedance** The input impedance at 5.8 GHz is 50 Ohms. The slight tail on the fifth element of the array provided a convenient adjustment and is at times used to improve the input impedance without a significant impact to the radiation patterns.

Series/Parallel Feed for Microstrip Array Antennas[24]

As the final example of microstrip antenna arrays, the combination of series and parallel feed techniques will be examined. The series/parallel feed is quite common due to flexibility in the ability to provide amplitude taper and phase progression. The 1-x-5 series feed array of the previous section is repeated four times to form a 4-x-5 array with amplitude taper in azimuth, and no amplitude taper in elevation. The results are graphically summarized in Table 9.

[24] The series fed array is also referred to as a traveling wave antenna.

TABLE 9: 4-X-5 ELEMENT LINEAR ARRAY WITH AZIMUTH AMPLITUDE TAPER

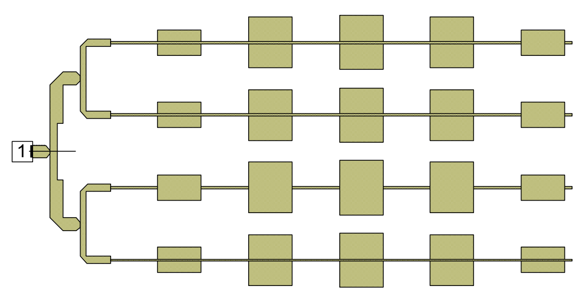

a. 4-x-5 Linear Array with Azimuth Amplitude Taper

Each row of the array is fed from the output of an equal amplitude power divider. As a result, each of the 1-x-5 composite arrays has an equal distribution in elevation.

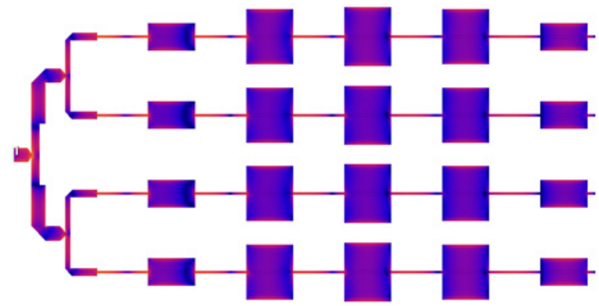

b. Conductor Current Distribution

The conductor current discloses near zero phase excitation. Note the slight advance of the phase excitation at the first element. The non-zero phase excitation contributes to pattern asymmetry.

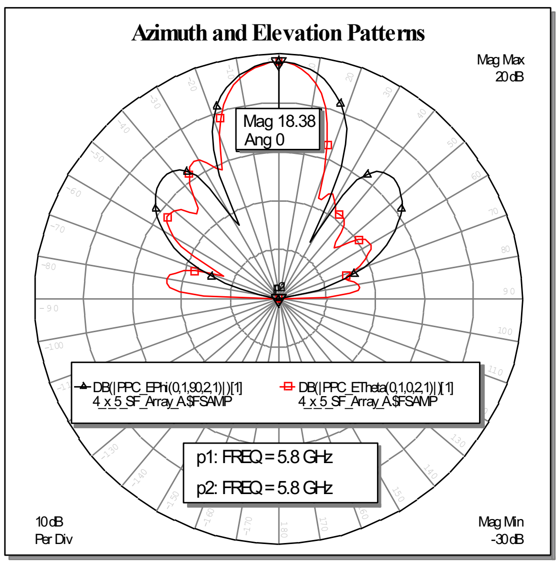

c. 4-x-5 Array Radiation Patterns

The lower sidelobe levels of the azimuth pattern (red) disclose the amplitude taper. The asymmetry of the azimuth pattern reflects the minor, non-zero phase excitation as evident from the conductor current. The expected gain increase of 6.0 dB over the 1-x-5 array is not realized due to power divider and conductor losses.

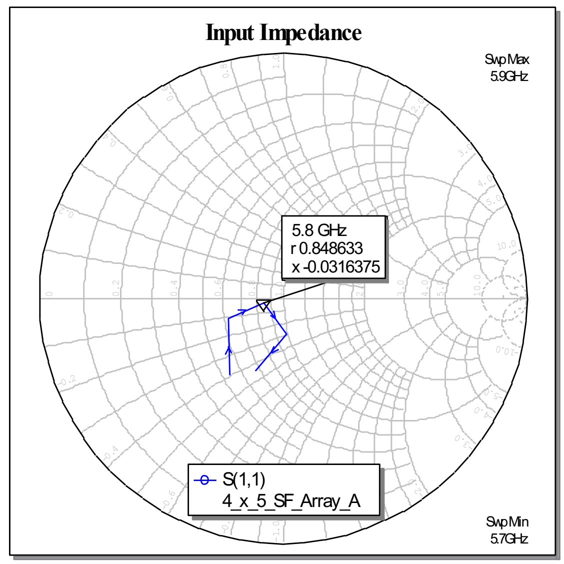

d. 4-x-5 Array Input Impedance

The 4-x-5 array input impedance appears well matched; the result of optimization of the 1-x-5 prior to elevation expansion of the array. The bandwidth of the matched impedance may be improved by adjusting the center frequency impedance point to the right in the 1_x-5 array. The input impedance at the band edges is improved with only a slight degradation to the center frequency impedance.

As a final example of microstrip antenna array properties, the previous 4-x-5 array performance is enhanced by amplitude taper in elevation to reduce the elevation beam sidelobes. The results are graphically illustrated in Table 10.

TABLE 10: 4-X-5 ELEMENT LINEAR ARRAY WITH AZIMUTH AND ELEVATION AMPLITUDE TAPER

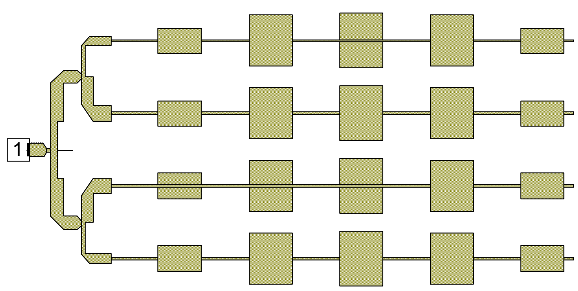

a. 4-x-5 Linear Array with Azimuth and Elevation Amplitude Taper

Each row of the array is fed from the output of an unequal amplitude power divider. As a result, the amplitude has an unequal distribution in elevation.

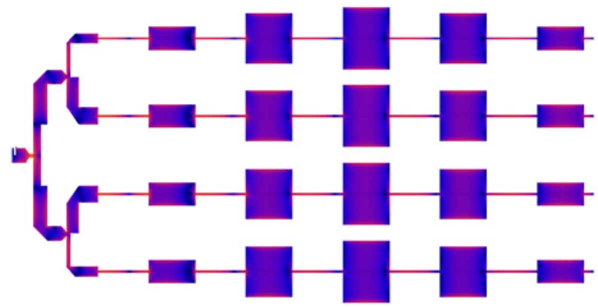

b. Conductor Current Distribution

The conductor current discloses near zero phase excitation. Note the reduced conductor current of the top and bottom rows of the array.

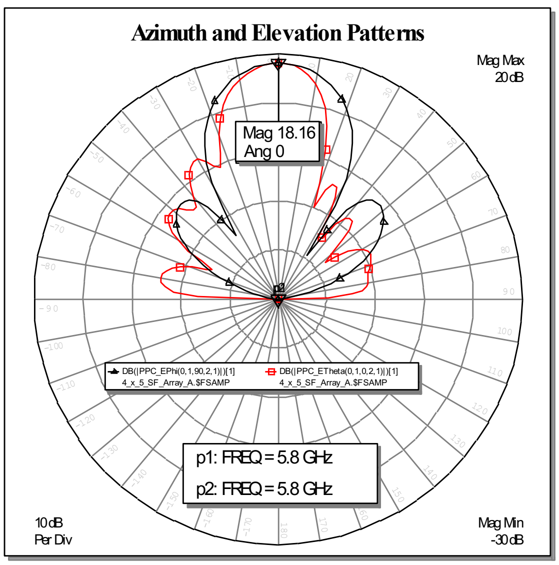

c. 4-x-5 Array Radiation Patterns

The lower sidelobe levels of both patterns reflect the two dimensional amplitude taper. The gain is slightly reduced from the equal power distribution of the previous array. In many applications, -20 dB sideband levels are acceptable.

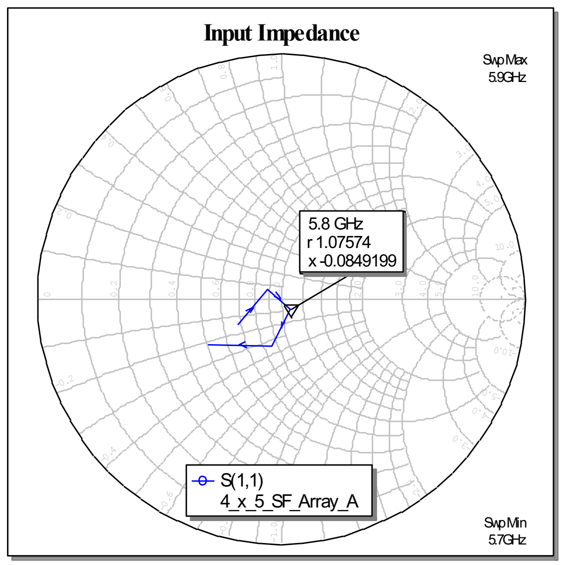

d. 4-x-5 Array Input Impedance

The 4-x-5 array input impedance appears well matched; the result of optimization of the 1-x-5 array prior to elevation expansion of the array. The bandwidth of the matched impedance may be improved by adjusting the center frequency impedance point to the right in the 1_x-5 array. The input impedance at the band edges is improved with only a slight degradation to the center frequency impedance.

Notwithstanding the flexibility and ease of incremental design and analysis, the series/parallel feed of microstrip array antennas is limited; particularly with respect to amplitude taper of the series feed elements. The limitation in magnitude of the amplitude distribution results directly from the limited sensitivity of the single element microstrip antenna to variation in conductor width, W. A quantitative evaluation of the sensitivity of microstrip antenna directivity may be attained via numeric evaluation of the single element directivity equation (equation 12) with W as a variable.

CONCLUSION

A judicious approach to the EM simulation of antenna arrays is represented in the incremental analysis structure; starting with a complete exploration of a single element of the array, and subsequently advancing to additional elements of the rows and columns. The investment of an incremental structure yields benefits in the form of reduced EM analysis time and improved correlation between expected and achievable performance – not to mention reducing the inherent anticipatory stress during simulation execution time.

The discussion related to microstrip antenna feed has been limited to that of the direct feed at the conductor edge, which results in limited operational bandwidth. The operational bandwidth of microstrip antennas may be significantly increased via implementation of an aperture coupling below the microstrip element; the improved performance is accompanied by the additional complexity and cost of a dielectric and conductor layer below the radiating elements.

REFERENCES

[1] Carver, K. R. and Minks, J. W., Microstrip Antenna Technology, IEEE Transactions on Antennas and Propagation, vol. AP-29, no. 1, January, 1981.

[2] Pozar, D. M. and Schaubert, D. H., *Microstrip Antennas*, IEEE Press, Piscataway, NJ, 1995.

[3] Balanis, C. A., *Antenna Theory*, 3rd Ed., John Wiley and Sons, Hoboken, NJ, 2005.

[4] Bahl, I. J. and Bhartia, P., *Microstrip Antennas*, Artech House, Dedham, MA, 1980.

[5] Bancroft, R., *Microstrip and Printed Antenna Design*, 2nd Ed., Scitech Publishing, Raleigh, NC, 2009.

[6] Stutzman, W. and Thiele G., *Antenna theory and Design*, 2nd Ed. John Wiley, NY, 1998.

[7] Antenna Design Associates, Inc., Introduction to Practical Antennas, PCAAD version 6, 2007.

Appendix A – Microstrip Antenna Analysis using PCAAD version 6.0 [7]

The numeric results of the microstrip antenna design example of Table IV were used as the input data for the PCAAD transmission line model software analysis. The PCAAD analysis is presented in Table A-I below. Note from the 'splash screen' results that the resonant frequency is predicted to be 5.7 GHz as opposed to the design center frequency of 5.8 GHz. The input impedance at resonance is 213 Ohms which is within acceptable limits considering the simplicity of the transmission line model. The directivity is predicted to be 7.0 dB which supports the calculated directivity of 7.0 dB and the EM simulation of gain result at 6.86 dB. The EM simulation result includes the effects of impedance mismatch loss and feed line impedance transformer loss.

Table A-I PCAAD Analysis Results of Microstrip Design Example

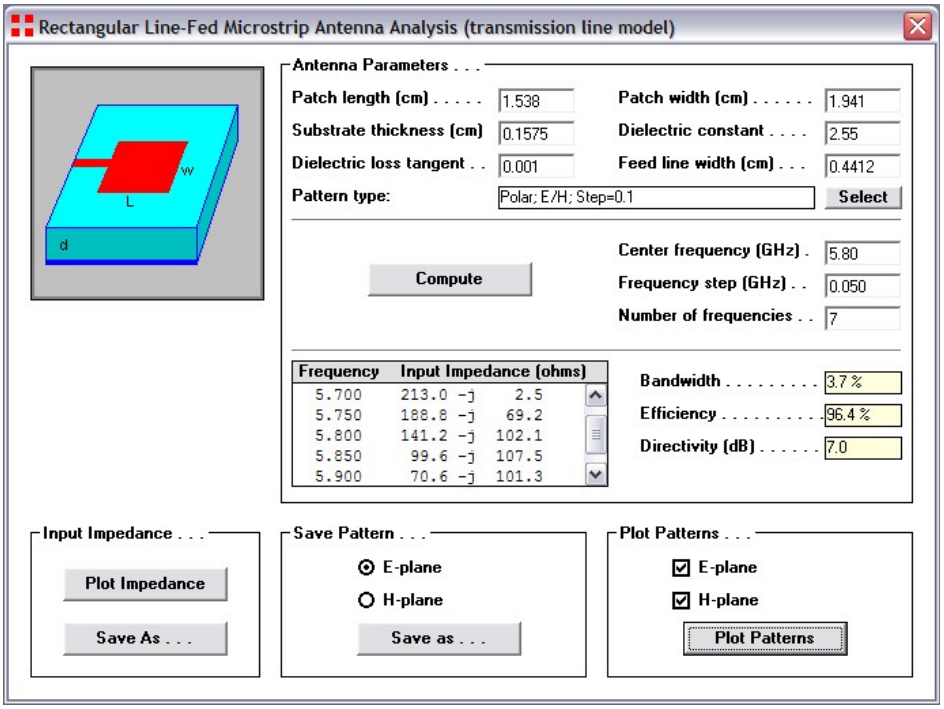

PCAAD 'Splash Screen' for Microstrip Antenna Design using Transmission line Model

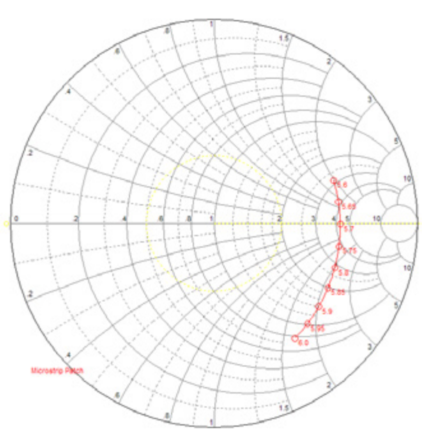

a. Input Impedance

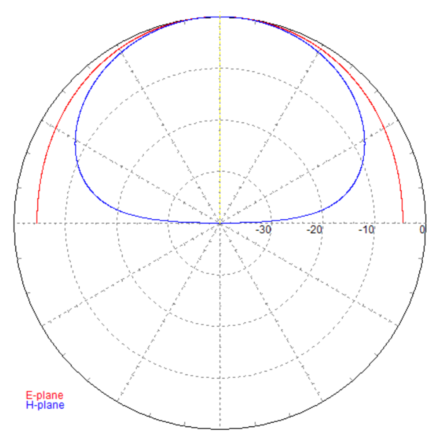

b. Radiation Patterns

APPENDIX B – ELECTROMAGNETIC RADIATION FROM A DIPOLE ANTENNA[25]

The prediction of electromagnetic wave propagation by James Clerk Maxwell, circa 1865, and subsequent experimental verification by Heinrich Hertz, circa 1887, is singularly, the most significant achievement of the 19th century. Prior to Maxwell's prediction and extensive documentation in "*A Treatise on Electricity and Magnetism*" (1873), electricity and magnetism consisted exclusively of isolated experimental observation by several noted scientists, among them: Coulomb, Ampere, Gauss, Volta and Faraday. Maxwell used his extraordinary insight and mathematical proficiency to produce a mathematically and scientifically definitive work which unified the subjects of electricity and magnetism and established the foundation for the study of electromagnetics.

Maxwell recognized the coupling and symmetry of the curl equations and concluded that the previously independent fields were, in fact, related.

Maxwell's Curl Equations for a charge free region:

$$\nabla \times \vec{E} = -\mu \frac{\partial \vec{H}}{\partial t}$$

$$\nabla \times \vec{H} = \varepsilon \frac{\partial \vec{E}}{\partial t}$$

The curl of a vector field may be physically interpreted as a mathematical operation which finds its source. Therefore, the curl of the electric field vector, i.e., $\nabla \times \vec{E}$, finds its source as the time derivative of the magnetic field vector; and conversely, the curl of the magnetic field vector, i.e., $\nabla \times \vec{H}$, finds its source as the time derivative of the electric field vector. One may extend the observations and further conclude that there exists a repeated, or periodic, cause-and-effect relationship between the coupled vector fields.

The action of the related fields may now be extended using a practical example. Consider Figure B-1, where a simple dipole element exists along the *z*-axis with current, I. The current is the result of a sinusoidal voltage source at the input terminals of the dipole.

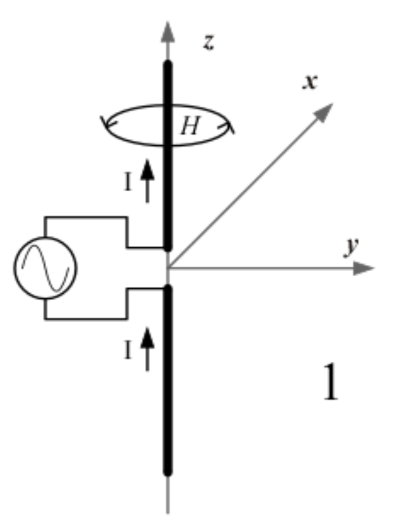

Figure B-1: Simple Dipole with Sinusoidal Excitation

(upon application of excitation, the current produces the *H*-field)

At the initial instant of application of the excitation source, the H-field is circumferential and lies in a plane which is normal to the axis of the diode. The current is assumed constant over the length of the diode and produces a magnetic field around the dipole element in accordance with Maxwell's equation:

$$\nabla \times \vec{H} = \vec{J}_c$$

Recall from the curl operation, the H-field has found its source, i.e., the current density along the dipole element, and that the geometrical relationship of the curl and its source is orthogonal.

As stated earlier, the time changing magnetic field vector – the source – produces an electric field vector in accordance with Maxwell's equation for a charge free region:

[25] The explanation is not scientifically or mathematically accurate; it is intended to offer a physical interpretation of the method by which electromagnetic waves originate in the proximity of a conductor carrying a sinusoidal current, and to subsequently propagate from the conductor.

$$\nabla \times \vec{E} = -\mu \frac{\partial \vec{H}}{\partial t}.$$

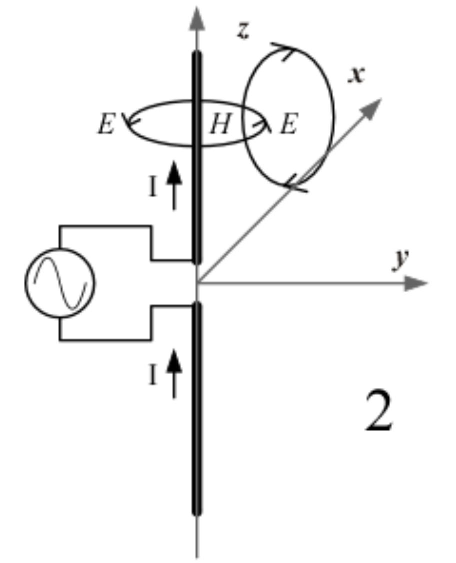

Figure B-2: Simple Dipole with Sinusoidal Excitation
(the initial *H*-field becomes the source of an *E*-field)

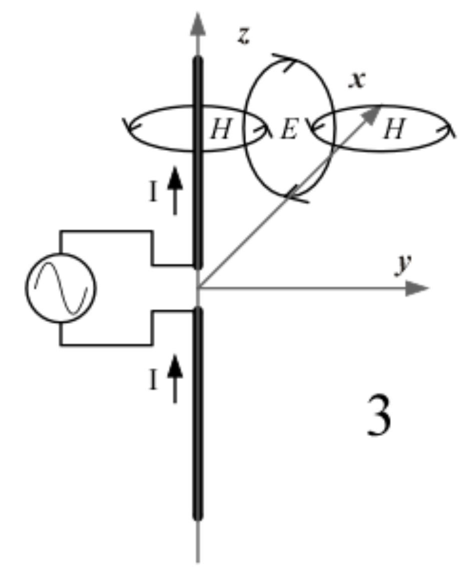

Figure B-3: Simple Dipole with Sinusoidal Excitation
(the time varying *E*-field is the source for the *H*-field)

Figures B-2 and B-3 illustrate the continuing progression and propagation of the EM wave from the dipole. The astute reviewer recognizes that the propagation is circumferentially symmetrical about the *z*-axis.

The initial premise for the generation and propagation of electromagnetic waves is the sinusoidal current on the diode element; more specifically, the acceleration and deceleration of charge within the conductor. Charges moving with a constant velocity do not produce electromagnetic waves. This principle is embodied within Maxwell's Equations which comprehensively describe and characterize the subject of electromagnetics – with the exception of relativistic effects.

An interesting property of electromagnetic waves is that, unlike sound, a medium is not required for propagation, and that the principal loss mechanism in free space is the spreading of the wave-front. The spreading loss may be visualized by the observation of a flashlight illuminating a surface while the surface is moved away from the light. The same amount of light, i.e., power, occupies a larger area and the power density is thereby reduced. There are other environmental EM wave loss mechanisms such as oxygen and water molecules which interact with an EM waves at particular frequencies. Other loss mechanisms are rain, ice and other particulate matter which might be encountered within the atmosphere.

The fact that no medium is required for EM wave propagation is particularly heartening when one considers the life-enabling EM radiation available from the sun.

Although the non-rigorous illustration of dipole radiation illustrates the *H*-field and *E*-field coupling as sequentially related, the field vectors for the plane-wave in free space are in-phase.

The power density of an EM wave at a point in space is the product of the normal components of the wave-front as represented by the Poynting vector:

$$\vec{P} = \left(\vec{E} \times \vec{H}\right) = \vec{a}_y \left|E_z\right| \cdot \left|H_x\right|$$

In this case, the geometry of the dipole example has been utilized such that the *E*-field polarization is z-directed while the *H*-field polarization is *x*-directed. The indicated cross-product is *y*-directed and the units are Watts/meter^2, clearly a power density. A similar expression for the power density along the *x*-axis may be written:

$$\vec{P} = \left(\vec{E} \times \vec{H}\right) = \vec{a}_x \left|E_z\right| \cdot \left|H_y\right|$$

Special thanks to Kenneth Puglia for developing the materials presented in this eBook. Puglia is the founder and principal engineer of E X H Consulting Services, an independent consultancy for radar sensors, frequency synthesis, up/down converters, and microwave subsystems and components. Prior to starting his own consultancy in 2009, he held numerous positions over his 38-year career with M/A-Com, including Fellow of Technology. Prior to joining M/A-Com, he was a design engineer with the Radio Corporation of America (RCA). Puglia is the author of numerous articles in industry trade magazines, including Microwave Journal. He graduated from University of Massachusetts, Lowell with a BSEE degree and received his MSEE from Northeastern University in 1971.

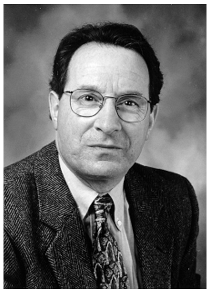

Kenneth Puglia, E X H Consulting Services